Nonlinear radiation imprisonment in magneto-optical vapor traps

N. N. Bezuglov,[1] A. F. Molisch,[2] F. Fuso,[3] M. Allegrini,[3,4] and A. Ekers[5]
[1]*V. A. Fock Institute of Physics, St. Petersburg University, 198904 St. Petersburg, Russia*
[2]*Department of Electroscience, Lund Technical University, Lund, Sweden*
[3]*Dipartimento di Fisica Enrico Fermi and CNISM, Università di Pisa, I-56127 Pisa, Italy*
[4]*CNR-INFM PolyLab, I-56127 Pisa, Italy*
[5]*Laser Centre, University of Latvia, LV-1002 Riga, Latvia*
(Received 12 February 2008; published 13 June 2008)

We analyze nonlinear radiation imprisonment (RI) effects in an optically thick vapor in different temperature regimes. An analytical approach is proposed to treat nonlinear decay problems. Special attention is paid to vapor samples having curvilinear geometries (cylinder, sphere) and being excited by a strong laser pulse. We derive a number of new formulas for different radiative trapping factors as functions of opacity and propose a general approach for RI evaluation allowing us to deal with samples both at room and low, or very low, temperatures, such as those customarily achieved in magneto-optical trap (MOT) experiments. As a result, we predict a "subnatural" decay of radiation escaping from cold vapors, which can be envisioned as the basis for a sensitive and reliable MOT diagnostic tool.

DOI: 10.1103/PhysRevA.77.063414 PACS number(s): 32.50.+d, 32.80.−t, 37.10.−x, 03.65.Sq

I. INTRODUCTION

If an excited atom is surrounded by absorbing atoms in the ground state at high enough densities, the resonance radiation will be absorbed and reemitted many times before it escapes from the gas volume. Radiation imprisonment (RI) plays an important role in various areas of physics [1,2]. In astrophysics and spectroscopy, in particular, it must be taken into account to correctly describe the spectra of celestial bodies [3] or fluorescent signals [2]. Most of the studies on RI deal with linear equations of radiative energy transfer and assume a homogeneous vapor as the absorbing medium; many conventional experiments involving RI have been treated in the past under similar assumptions. However, several emerging experimental situations involve spectral emission and absorption coefficients that can be both spatially nonuniform [4,5] and nonisotropic [6], as, for instance, in low-temperature atomic samples (MOTs and atom beams). Moreover, the RI problem becomes strongly nonlinear if the excitation of the atomic vapor is produced by a laser pulse sufficiently strong to saturate the resonance transition [7,8]. Under such conditions, the optical thickness of the medium becomes dependent on the density of excited atoms and the solution of radiation trapping equations appears to be challenging. Some methods for treating heterogeneous and nonlinear RI problems have been elaborated for astrophysical applications [3], but they are restricted mainly to steady state conditions, flat geometries (e.g., atmospheres of planets) and an assumption of complete frequency redistribution (CFR) of the reemitted radiation.

As pointed out in recent decades, RI is involved in important heating and loss channels of atoms in MOTs [9], preventing attainment of arbitrarily low temperatures [10]. Both the spherical geometry of MOTs and the large intensity of lasers used in manipulating atoms require considering the specific behavior of RI in cold samples with nonflat geometries, which cannot be properly described by conventional methods. Investigations of RI in MOTs both under time-dependent [4,11,12] and steady-state conditions [5] have been reported. The results, however, were actually related to the linear regime of radiative energy transfer. In fact, although intensities of probe lasers used in [4,11] were large enough to access the nonlinear regime, the authors restricted themselves mainly to the late stage of excitation decay, where the corresponding regime can be considered as truly linear. It is important to point out that the development of a nonlinear treatment for RI in MOTs offers the additional benefit of a reliable diagnostic tool, potentially able to determine the particle density of the sample without the limitations offered by conventional methods (e.g., absorption measurements or techniques based on the evaluation of decay time constants at the late stage of the process). Even if the spectroscopic features of cold vapors have been extensively investigated in the past, to the best of our knowledge nonlinear fluorescence decay processes have not been clearly identified in experiments, nor predicted by accurate approaches accounting for the specific geometrical and spectral conditions of the cold vapor. This provides us with a strong motivation to develop an analytical approach allowing an adequate modeling of the nonlinear processes.

A general method, the so-called geometrical quantization technique (GQT), was proposed by us to describe linear RI problems in optically dense vapors and plasmas with uniform [13,14] and nonuniform [15,16] spatial distributions of the absorbing and emitting centers. In particular, we exploited GQT to analyze RI processes in MOT conditions with partial frequency redistribution (PFR) in reemission events using the theory suggested in [17]. Another analytical approach to treat time-dependent nonlinear problems was developed in [8] (hereafter referred to as paper I) and was considered mainly in its application to a flat absorbing layer at room temperature and under the CFR. Although it was pointed out in paper I that this was an approach suitable to deal with cylindrical and spherical geometries, the corresponding cases were only briefly mentioned. The aim of the present paper is threefold: (i) We intend to provide a consistent description of simple analytical approaches (outlined in

paper I) in a form suitable for modeling nonlinear RI processes in curvilinear geometries, suitable for atomic beams, cylindrical plasmas, and spherical MOT configurations; (ii) thanks to improvements in the numerical codes used for solving RI equations [18], we present results able to describe the specific conditions of experiments in MOTs considered in [4] (hereafter referred to as paper II) with improved accuracy; (iii) based on numerical simulations, we discuss the occurrence of the so-called subnatural decay of fluorescence signal [7,8] in low-temperature atomic samples, i.e., we identify reasonable conditions expected to lead, upon pulsed excitation, initially to a very fast decay, corresponding to effective decay constants Γ_{eff} significantly larger than the natural decay rate, Γ.

The work is organized as follows: In Sec. II, we define the problem and give its mathematical description in the form of a nonlinear RI equation of the Holstein-Biberman-Payne type. This equation describes the evolution of the excited state population $n^*(\vec{r},t)$ of the atoms within the sample; we also point out how to modify the formalism to recover the master equation of RI in MOTs. Section III briefly summarizes the results of paper I along with their modifications to account for MOT conditions (Sec. III B): We introduce two reduced equations allowing approximate analytical solutions for $n^*(\vec{r},t)$ averaged over the whole sample volume, and over the initially excited region, respectively, and we determine the corresponding correction factors needed to accurately evaluate the involved quantities (Sec. III A). Section III C addresses the issue of finding *ab initio* correction factors for the reduced equations accounting for the vapor geometry. In Sec. IV A we demonstrate the accuracy of our analytical method by comparing its predictions with numerical results for the case of samples with cylindrical geometry and room temperature. Then we discuss (Sec. IV B) the phenomena of fast (subnatural) decrease of photon flux emerging from a sample operated under typical MOT conditions and derive a simple equation to obtain analytical solutions for flux evolution. The Appendix contains details of a mathematical treatment of some features of escape factors related to conditions of MOT experiments.

II. FORMULATION OF THE PROBLEM

We are interested in the following situation: A strong laser pulse excites the central part, region A with boundary S_A, of a vapor sample with total volume Ω (see Fig. 1) and radius R. If Ω has a flat geometry [Fig. 1(b)], R corresponds to its half-width. The intensity of the laser is assumed to be sufficiently large to produce an almost complete saturation of the resonance transition in region A. This means that the stimulated emission becomes practically equal to the absorption, so that the effective absorption in region A becomes close to zero. Our main attention will be focused on the so-called afterglow regime, i.e., we will investigate the vapor in the time interval after the end of the saturating pulse. As time passes, more and more excited atoms situated in A will decay to the ground state, so that the effective absorption coefficient increases. However, some of the fluorescence photons are reabsorbed, which tends to balance the increase in the

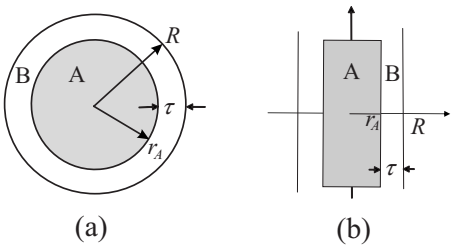

FIG. 1. Scheme of the geometries for the vapor medium Ω considered in the text: Region A is directly excited by a strong laser pulse; the parameter $\rho=r_A/R$ gives the relative size of the excitation zone. Region B is assumed to be initially nonexcited so that the vapor opacity τ is concentrated initially in region B. (a) Curvilinear configuration (a cylinder or a sphere). (b) Linear configuration (a flat layer or a slab).

effective absorption coefficient. Such cross linking causes a strong nonlinearity in the radiative transfer equation coupled with the rate equations of atomic level population.

All of the above features can be accounted for under the model of a two-level atom within the frame of conventional Holstein-Biberman-Payne (HBP) theory [1,20,21]. The approach allows for incorporating both the rate equations and light-vapor interaction into one nonlinear kinetic integral equation governing the evolution of the ground-state $n_1(\vec{r},t)$ and excited-state $n^*(\vec{r},t)$ densities. In presenting the HBP equation we will follow the notations adopted in paper I. The effective spectral absorption coefficient $\kappa(\nu,n^*)$, which describes the difference between absorption and stimulated emission, plays a prominent role in describing the process. It clearly depends on the ground-state and excited-state densities which in turn depend on the spatial coordinate $\vec{r}$ and on the time t,

$$\kappa(\nu,\vec{r}) = \kappa_0 \theta_\nu n_1(\vec{r},t)\left(1 - \frac{n^*(\vec{r},t)}{n_1(\vec{r},t)}\frac{g_1}{g^*}\right), \tag{1}$$

where g_1 and g^* are the statistical weights of the ground and of the excited state, respectively, κ_0 is the absorption coefficient per unit atom in the center of the absorption line, ν_0, and the absorption line shape θ_ν satisfies $\theta_{\nu=\nu_0}=1$.

The behavior of the profile θ_ν in the line wings strongly affects the photon trapping effects. According to the quasistatic theory of the spectral line broadening, the decrease of θ_ν in the wings is ruled by a power-law function [3,19], $\theta_\nu \sim |\nu-\nu_0|^{-\mu}$. Three situations, corresponding to Doppler, Lorentz, and mixed profiles, are relevant to describe most experiments,

$$\kappa_D(\nu) = \kappa_0^{(D)} \exp(-\nu_D^2), \quad \nu_D = \frac{\nu-\nu_0}{\Delta\nu_D},$$

$$\kappa_0^{(D)} = \frac{\lambda^2}{8\pi^{3/2}}\frac{\Gamma}{\Delta\nu_D}\frac{g_1}{g^*}n,$$

$$\kappa_L(\nu) = \kappa_0^{(L)}(1+\nu_L^2)^{-1}, \quad \nu_L = \frac{\nu-\nu_0}{\Delta\nu_L}, \quad \kappa_0^{(L)} = \frac{\lambda^2}{8\pi^2}\frac{\Gamma}{\Delta\nu_L}\frac{\bar{g}_1}{\bar{g}_2}n,$$

$$\kappa_v(\nu) = \frac{a}{\pi}\int_{-\infty}^{\infty} \frac{\exp(-y^2)}{a^2+(\nu-y)^2}dy, \quad \nu = \frac{\nu-\nu_0}{\Delta\nu_D}, \quad a = \frac{\Delta\nu_L}{\Delta\nu_D},$$

$$\kappa_{\mathrm{MOT}}(\nu) = \kappa_0^{(M)}(1+\nu_L^2)^{-1}, \quad \nu_L = \frac{\nu-\nu_0}{\Delta\nu_L}, \quad \kappa_0^{(M)} = \frac{\lambda^2}{2\pi}\frac{\bar{g}_1}{\bar{g}_2}n, \tag{2}$$

$\kappa_0^{(D)}$ and $\kappa_0^{(L)}$ being the absorption coefficient at line center ν_0 for the Doppler and Lorentz lines with widths $\Delta\nu_D$ and $\Delta\nu_L$. The total density $n=n^*+n_1$ of vapor atoms is assumed to be independent of position. In the Voigt case, the absorption coefficient is expressed as $\kappa_0=\kappa_0^{(D)}$. Formally, the exponential dependence of the Doppler profile can be recovered by placing $\mu=\mu_D=\infty$. Noteworthy, under the MOT conditions of paper II, the absorption line corresponds to the Lorentz one [see the fourth line in Eq. (2)], i.e., the absorption power index $\mu=\mu_{\mathrm{MOT}}^{(ab)}=\mu_L=2$ (but the power index $\mu_{\mathrm{MOT}}^{(em)}=6$ for an emission line in an optically dense MOT, as we will discuss in the following).

As already stated, the initial conditions are given by assuming strong saturation of the optical transition in region A at the end of the exciting laser pulse ($t=0$): The excited atom density n_A^* becomes then a noticeable fraction of the total density n,

$$n_A^* = Pn_S^*, \quad n_S^* \equiv n\frac{g^*}{g_1+g^*}, \tag{3}$$

where n_S^* corresponds to the complete saturation value of the resonance state. Thus, according to Eq. (1), the effective absorption by the vapor vanishes, and $\kappa(\nu,n_S^*)=0$ in the region A provides the saturation parameter $P=1$. In order to deal with one-dimensional problems, we assume that the region A is placed always in the center of the volume Ω. It is convenient to express its size, the radius r_A (see Fig. 1), in R units by introducing the nondimensional geometrical parameter $\rho=r_A/R$.

The opacity χ between two points $\vec{r},\vec{r}'$, separated by the distance $\rho=|\vec{r}-\vec{r}'|$ is given by the integral

$$\chi(\nu,\vec{r},\vec{r}';n^*) = \int \kappa(\nu,\vec{r}_l)dl \tag{4}$$

calculated over a straight line (with the current coordinate $\vec{r}_l$) connecting $\vec{r}$ with $\vec{r}'$. The probability G that a photon emitted at $\vec{r}'$ is reabsorbed at $\vec{r}$ depends on the variables introduced above according to [20,21],

$$G(\vec{r},\vec{r}';n^*) = \frac{1}{4\pi\rho^2}\int \kappa(\nu,\vec{r})\varphi(\nu,\vec{r}')\exp[-\chi(\nu,\vec{r},\vec{r}';n^*)]d\nu. \tag{5}$$

The spectral function $\varphi(\nu,\vec{r}')$ determines the frequency distribution of emitted photons and is normalized by $\int\varphi(\nu,\vec{r}')d\nu=1$. We note that the expression (5) contains photon variables and allows for formulating the balance (Holstein) equation for atoms in a closed form,

$$\frac{\partial n^*(\vec{r},t)}{\partial t} = -\Gamma n^*(\vec{r},t) + \Gamma\int_\Omega G(\vec{r},\vec{r}';n^*)n^*(\vec{r}',t)d^3r'. \tag{6}$$

Indeed, the excited-state density n^* is decreased by the natural decay occurring at the rate Γ. On the other hand, n^* is increased by reabsorption of photons that are emitted somewhere else (at the point $\vec{r}'$) in the vapor. As a result, the second (integral) term contains reabsorption probability G as the kernel of the (nonlinear) integro-differential equation. The nonlinear behavior occurs due to the dependence of the opacity χ on n^* [see Eqs. (1) and (4)].

Under the conventional model of complete frequency redistribution of reemitted photons used in Holstein-Biberman theory (see [2] for details), the emission profile $\varphi(\nu)$ is assumed to be proportional to the absorption profile θ_ν and, thus, does not depend on spatial coordinates. The more general Payne treatment [21] deals with a partial frequency redistribution (PFR) function for reemission processes, but it is reduced to the Holstein equations (5) and (6) provided one can obtain information (from an experiment or computer simulations) on $\varphi(\nu)$ [14]. The case of PFR under MOT conditions was studied in paper II. Because of very small atom velocities typical for subthermal samples, the absorption line shape $\kappa_{\mathrm{MOT}}(\nu)$ is described by the conventional Lorentzian function $\kappa_L(\nu)$, Eq. (2) (the fourth line), with $\Delta\nu_L=\Gamma/4\pi$. The emission profile $\varphi_p(\nu)$, however, turns out to exhibit a specific explicit form

$$\varphi_p^{(\mathrm{MOT})}(\nu) \sim \frac{\lambda_p}{\pi}\frac{1}{1+\nu^2}\frac{1}{V_p(\nu)},$$

$$V_p(\nu) = 1 - \frac{\kappa_L(\nu)}{p}\arctan\left(\frac{p}{\kappa_L(\nu)}\right), \tag{7}$$

which depends on the MOT opacity $\tau=\kappa_0^{(M)}R$ via the parameter p determined in paper II,

$$\lambda_p^{-1} \equiv \frac{1}{\pi}\int_{-\infty}^{\infty}\frac{d\nu}{1+\nu^2}\frac{1}{V_p(\nu)}, \tag{8}$$

$$\tau = \frac{\Delta S(p)+\pi}{2p/\kappa_0^{(M)}}, \quad \Delta S(p) = \frac{\pi}{2}\left[1+\frac{1}{2}p\frac{d}{dp}\ln\left(p\frac{d\lambda_p}{dp}\right)\right]. \tag{9}$$

Equation (9) gives the functional relation between values p and τ. The function $V_p(\nu)$ can strongly modify the Lorentzian behavior of the MOT emission profile. For small opacities, $p\to\infty$, so that $\varphi_p^{(\mathrm{MOT})}(\nu)$ coincides with the $\kappa_L(\nu)$ profile, while in the region of large τ ($p\to 0$), $\varphi_p^{(\mathrm{MOT})}$ acquires a quite different behavior,

$$\varphi_{p\sim\infty}^{(\mathrm{MOT})}(\nu) \cong \frac{1}{\pi}\frac{1}{1+\nu^2}, \quad \varphi_{p\sim 0}^{(\mathrm{MOT})}(\nu) \cong \frac{8}{3\pi}\frac{1}{(1+\nu^2)^3}. \tag{10}$$

In the wings, $\varphi_{p\sim 0}^{(\mathrm{MOT})}(\nu)\sim|\nu-\nu_0|^{-6}$ [4], i.e., as already anticipated, $\mu_{\mathrm{MOT}}^{(em)}=6$. In the following (Sec. IV B) we will analyze in more detail the consequences of such a peculiar dependence of the absorption and emission profiles in the fluorescence emission from a MOT sample.

Equation (6) is a master equation determining all experimentally observable variables, related to both atomic levels and the fluorescence signal (see Sec. IV). In completing the description of our theoretical background, we recall the set of the main (not very restrictive) assumptions needed in the following (paper I contains a more detailed discussion). It is required that (i) the whole region A is excited homogeneously; (ii) a two-level atom model is applicable; (iii) collisional quenching and broadening are negligible; (iv) the emission profile is independent of position; (v) the laser pulse must be shorter than the radiative lifetime Γ^{-1}; (vi) the laser pulse must be strong enough to cause appreciable saturation of the resonance transition in the excitation of region A. Since we consider the afterglow stage of the experiment, high-field effects (e.g., ac-Stark splitting) are expected to be negligible.

III. REDUCED TRAPPING EQUATIONS

The time-dependent, nonlinear equation (6) can be solved in its general form via numerical simulation only. If we restrict ourselves to some integrated features of the excited states, namely the total numbers $N^*(t)$ and $N_A^*(t)$ of excited atoms in the region Ω (with volume V_Ω) and in the region A (with volume V_A), it is possible to substantially simplify the treatment. In this section we briefly discuss the reduced equations for determining $N^*(t)$ and $N_A^*(t)$ according to the method presented in [8]. Special attention is paid to describing a number of correction factors in kinetic coefficients which account for different regimes in the decay processes of the initial excitation. Our main aim is to extend the results of paper I in order to derive the proper construction of the reduced equations allowing sufficiently accurate solutions for $N^*(t)$ and $N_A^*(t)$ for curvilinear geometries and under MOT conditions.

The relevant rate equations including all correction factors can be written as

$$\frac{dN^*}{dt} = -\Gamma \vartheta_{ef}^{(H)}(\tau(t)) \cdot N^*(t), \tag{11}$$

$$\tau(t) \equiv \tau(N^*(t)) = \tau^{(M)}\left(1 - \frac{N^*(t)}{n_S^* V_\Omega}\right)\left(1 + \frac{N^*(t)}{n_S^* V_A}\Delta\right),$$
$$\tau^{(M)} = n\kappa_0 R, \tag{12}$$

$$\frac{dN_A^*(t)}{dt} = -\Gamma \vartheta_{ef}^{(H)}(\tau_A(t)) \cdot N_A^*(t) + \Gamma(N^* - N_A^*)\vartheta_{ex}(\tau_A(t)\eta)\eta^{-1}, \tag{13}$$

$$\tau_A(t) \equiv \tau_A(N_A^*(t)) = \tau_A^{(M)}\left(1 - \frac{N_A^*(t)}{n_S^* V_A}\right)\left(1 + \frac{N_A^*(t)}{n_S^* V_A}\Delta_A\right),$$
$$\tau_A^{(M)} = n\kappa_0 r_A. \tag{14}$$

Equations (11) and (13) must be combined with the initial conditions $N^*(t=0)=N_A^*(t=0)=Pn_S^*V_A$ according to Eq. (3). Importantly, Eqs. (11)–(14) were originally obtained under some simplifying assumptions without correction factors, i.e., with parameters $\Delta=\Delta_A\equiv 0$ and $\eta\equiv 1$. In what follows, we shall discuss in detail the nature of both balance equations (11) and (13) and the correction factors.

TABLE I. Correction factors Δ for different geometries.

	Layer	Cylinder	Sphere
	$k=1$	$k=2$	$k=3$
Δ_ρ	$0.27\ (1-\rho)$	$0.43(1-\rho^2)$	$0.57(1-\rho^3)$
Δ_G	0	$-0.4\rho^2$	$-(5/9)\rho^3$
Δ	Δ_ρ	$\Delta_\rho+\Delta_G$	$\Delta_\rho+\Delta_G$
Δ_A	0	-0.4	$-5/9$

The rate equation (11) has the form of the decay equation for N^* with an effective constant $\Gamma\vartheta_{ef}^{(H)}$ corresponding to the inverse Holstein g_0 factor [2,20]. In other words, $\Gamma\vartheta_{ef}^{(H)}$ coincides with the effective decay rate of the fundamental mode for the trapping equation in a vapor with total optical opacity $\tau(t)$. The physical meaning of Eqs. (11) and (12) is as follows. The effective decay rate of excited atoms depends on the current sample opacity $\tau(t)$, which, in turn, is determined by the current value of $N^*(t)$ via Eq. (12). If the initial saturation was complete, i.e., the excitation of the MOT vapor by the laser pulse has reached the maximum allowed value $N_s^*=n_S^*V_\Omega$ [see Eq. (3)], the sample would become transparent, with $\tau(t=0)=0$. For low excitation power, $N^*(t)/N_s^* \ll 1$, as is realized at a later stage of the decay process, the opacity $\tau(t)$ acquires its maximum value $\tau^{(M)}=n\kappa_0 R$.

An effective analytical method to evaluate $\vartheta_{ef}^{(H)}$ factors was suggested in [13] under the assumption of CFR and using the geometrical quantization technique,

$$\vartheta_{ef}^{(H)}(\tau) = \tilde{\lambda}_p \equiv \int_{-\infty}^{\infty} d\nu\varphi(\nu)V_p(\nu), \quad \tau = \frac{\Delta\tilde{S}(p) + 0.5\pi(k-1)}{2p/\kappa_0}. \tag{15}$$

The parameter k describes here the type of geometry: $k=1$ for a plane-parallel slab of total thickness $2R$; $k=2$ for a cylinder with radius R; $k=3$ for a sphere with radius R (see also Table I). The function $V_p(\nu)$ was introduced above, via Eq. (7), while $\Delta\tilde{S}(p)$ is obtained with Eq. (9) provided one exchanges $\lambda_p \to \tilde{\lambda}_p$. We note that $\vartheta_{ef}^{(H)}$ depends on τ due to dependence $\tau(p)$ involved in Eq. (15).

The methods of [13] were further developed in paper II where it was shown that under MOT conditions the Holstein effective rate constant $\vartheta_{\mathrm{MOT}}^{(H)}$ has the following analytical representation:

$$\vartheta_{ef}^{(H)} = \vartheta_{\mathrm{MOT}}^{(H)} = \lambda_p \tag{16}$$

with the dependence on the MOT opacity being given by Eqs. (8) and (9), which evidently differs from the previously introduced equation (15).

Considering Eq. (13) for a total excitation N_A^* of volume A, we notice that it has the form of a balance equation. The right-hand side of Eq. (13) consists of two terms. The first

one is the rate at which N_A^* decreases because of the photons leaving the region A [at the current opacity $\tau_A(t)$]. The second term corresponds to photons that are emitted in region B (from secondary-excited atoms) and are then reabsorbed in region A. The coefficient ϑ_{ex}, thus, plays the role of "interaction" constant between the excitation of regions A and B, and has a form different from that of $\vartheta_{ef}^{(H)}$ [8],

$$\vartheta_{ex}(\tau) = \frac{2^{1-k/2}}{k\Gamma(k/2)} \int_0^\infty d\nu \varphi(\nu) \frac{\tau\theta_\nu}{\kappa_0} \int_{\tau\theta_\nu/\kappa_0}^\infty dz z^{k/2-1} K_{k/2-1}(z). \tag{17}$$

The function K_μ is the modified Bessel function of the second kind, while $\Gamma(x)$ corresponds to the Euler Γ function [22]. MOT conditions can be recovered by applying Eq. (7) for the emission profile $\varphi(\nu)$ and by setting the value $k=3$ (spherical geometry).

The key point of paper I was the possibility to relate the current values of opacities $\tau(t)$ and $\tau_A(t)$ to the total numbers of atoms $N^*(t)$ and $N_A^*(t)$ via formulas of the kind

$$\tau(N^*) = \tau^{(M)}\left(1 - \frac{N^*}{N_S^*}\right). \tag{18}$$

However, strictly speaking, this relation is valid for a plane-parallel slab only (the $k=1$ case) where the so-called technique of reduced optical opacities [3] works well.

A. Correction factors

In order to apply Eq. (18) to cylinders and spheres, one needs to insert some corrections having the form of an additional multiplier $[1+N^*\Delta/(n_S^* V_A)]$ accounting for both specific features of curvilinear geometries (see below) and different aspects of nonlinear decay processes. Analytical representation of the correction factor Δ may be found *ab initio* by solving a set of reference problems. We shall illustrate this statement and consider in detail the derivation of formulas for the geometrical factor Δ_G (see Sec. III C). However, we will first discuss and make relevant comments on three basic types of correction factors displayed in Table I and affecting the factor η in Eq. (13).

The first type of corrections (the first line Δ_ρ in Table I) relates to the single-mode approach. It is well known [2] that if the initial excitation is localized sharply inside the volume Ω, the fluorescence decay process must involve a set of modes showing different effective radiative constants. Equation (11), in contrast, predicts a single-exponential decay of excitation (at least in the linear limit for small values of the saturation parameter P) corresponding to the fundamental mode of the spatial distribution of excited atoms. Single mode decay is typical when $\rho=r_A/R\simeq 1$, i.e., when the laser excites the majority of atoms in Ω. If the initially excited atoms were concentrated near the sample center ($\rho\simeq 0$), the decay, at early times, occurs on a slower time scale than predicted by Eq. (11). In order to recover the proper behavior of $N^*(t)$, we must increase the optical opacity τ in Eq. (18) by a factor Δ_ρ, $\tau(N^*)\to\tau(N^*)(1+\Delta_\rho)$. At later stages of decay, however, only the fundamental mode survives, so the above correction Δ_ρ must be switched off at some time. The following replacement,

$$\tau(N^*) \to \tau^{(M)}\left(1 - \frac{N^*}{N_S^*}\right)\left(1 + \frac{N^*}{n_S^* V_A}\Delta_\rho\right), \tag{19}$$

entering in Eq. (11) provides the proper dynamic interpolation at intermediate times. The values of Δ_ρ were derived in paper I from *ab initio* positions and are presented in Table I. Note that no corrections are needed for single-mode decays ($\rho\simeq 1$). The multiplier $(1-\rho^k)$ in Δ_ρ cancels the correction for such ρ values.

The second type of correction has a similar origin but relates to the excited atom distribution $n_B^*(\vec{r})$ in region B (see Fig. 1). The "coupling" constant ϑ_{ex} [Eq. (17)] accounting for excitation of atoms in region A by reemitted photons in region B implies that the distribution n_B^* is concentrated near the boundary of the central region A (see paper I). Such a picture, valid at early times, is no longer true when the fundamental mode starts determining the atom distribution in volume Ω; that requires a dynamic correction of the form

$$\vartheta_{ex}(\tau_A(t)) \to \vartheta_{ex}(\eta\tau_A(t))\,\eta^{-1}. \tag{20}$$

It turns out that this replacement does not affect the N_A^* curves when no correction is needed. Indeed, at the beginning of the decay when $x=\eta\tau_A(t)<1$, the function $\vartheta_{ex}(x)\sim x$ has a linear dependence on its argument [it follows directly from Eq. (17)] and, hence, the dependence on η in Eq. (20) is cancelled out. In contrast, the η factor influences strongly the value of ϑ_{ex} for large $\tau_A(t)$. A proper choice of η thus allows one to account for the spatial diffusion of excited atoms occurring due to radiation trapping processes in region B. The Appendix reports the details for the evaluation of the correction factor covering the three geometries under consideration for samples at room temperature,

$$\eta^{1+2\gamma}(1-\rho^{2\gamma}) = \left(\frac{N^*}{N_A^*} - 1\right)\frac{\vartheta_{ex}(\infty)}{\vartheta_{ef}^{(H)}(\infty)}\Lambda_k(\tau_A^{(M)}), \quad \Lambda_k(\tau_A^{(M)}) = \frac{\vartheta_{ex}(\tau_A^{(M)})}{\vartheta_{ef}^{(H)}(\tau_A^{(M)})}\frac{\vartheta_{ef}^{(H)}(\infty)}{\vartheta_{ex}(\infty)}, \tag{21}$$

$$N_A^* = F(\rho) \equiv \int_0^{\rho R} dr r^{k-1} n_H^*(r), \quad N^* = F(\rho=1),$$

$$n_H^*(r) = (1 - r^2/R^2)^\gamma. \tag{22}$$

A universal method for fast evaluation of $\vartheta_{ef}^{(H)}$ for flat layers ($k=1$), cylinders ($k=2$), and spheres ($k=3$) at room temperature was developed in [13] and summarized in Eq. (15). Importantly, both factors $\vartheta_{ex}(\tau)$ and $\vartheta_{ef}^{(H)}(\tau)$ have the same behavior $\vartheta(\tau)\sim\tau^{-2\gamma}$ at large opacities [3,13], so that the functions $\Lambda_k(\tau)$ have the asymptotic values $\Lambda_k(\tau=\infty)=1$. Under the assumption of complete frequency redistribution, the spectral parameter γ involved in Eq. (21) is determined by the wings of the line profile

$$\gamma = (\mu - 1)/(2\mu), \tag{23}$$

and it has values $\gamma_L=0.25$ ($\mu_L=0.5$) and $\gamma_D=0.5$ ($\mu_D=\infty$) for Lorentz and Doppler profiles, respectively. Furthermore, the spatial dependence $n_H^*(r)$ of the Holstein fundamental mode of decay is determined as well by the parameter γ, $n_H^*(r)$

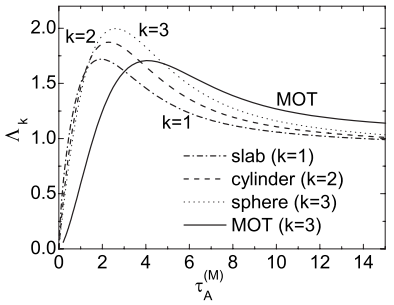

FIG. 2. Behavior of Λ_k factors as a function of the opacity $\tau_A^{(M)}$. The solid curve corresponds to the MOT function determined by Eq. (26). Other curves are evaluated via Eq. (21) and relate to different configurations of vapor volumes at room temperature: (i) A sphere ($k=3$); (ii) a cylinder ($k=2$); (iii) a flat slab ($k=1$). Λ_k factors achieve a unit asymptotic value at infinity for all the considered configurations.

$\sim(1-r^2/R^2)^{\gamma}$. This fact allows us to evaluate easily the ratio N^*/N_A^* entering Eq. (21). We stress that the function Λ_k reflects the dependence of λ factors on the opacity of region A and depends on the geometry type via the escape factors. Figure 2 shows the values of Λ_k as a function of the opacity $\tau_A^{(M)}$ for different types of geometry in the case of a Doppler profile. As demonstrated in paper I, the Doppler profile represents a reference case for all spectral profiles with extended wings and a divergent (infinite) value of photon mean free path. For this reason, in Eqs. (21) and (22) the Doppler value $\gamma=0.5$ can be used to obtain important information on the behavior of the Λ_k function, including the already mentioned asymptotic value $[\Lambda_k(\tau=\infty)=1]$. Table II shows the ratio $\vartheta_{ex}(\infty)/\vartheta_{ef}^{(H)}(\infty)$ entering Eq. (21).

B. Modifications for low-temperature samples

The discussion presented in the preceding section, where a Doppler profile has been explicitly considered, is successful in providing results valid for a wide variety of geometries, but it fails in describing the peculiar behavior of low-temperature samples. Since our goal is to reliably predict RI in cold samples, in particular those realized in a MOT, we must take into account specific modifications. We start noting that, as discussed above, the correction represented by the factor η implies that functions $\vartheta_{ex}(\tau)$ and $\vartheta_{ef}^{(H)}(\tau)$ have similar asymptotes $\vartheta(\tau\to\infty)\sim\tau^{-2\gamma}$. In low-temperature samples, i.e., in a MOT, the CFR assumption is no longer valid, which manifests itself in quite different values of wing indices μ_{MOT} for absorption ($\mu_{\mathrm{MOT}}^{(ab)}=2$) and emission ($\mu_{\mathrm{MOT}}^{(em)}=6$) profiles at high opacities. By assuming a spherical geometry ($k=3$), an essential simplification of Eq. (17) can be achieved,

TABLE II. The ratio $P=\vartheta_{ex}(\infty)/\vartheta_{ef}^{(H)}(\infty)$ for different geometries.

	Layer	Cylinder	Sphere
	$k=1$	$k=2$	$k=3$
P	1/1.82	$\pi/12.6$	1/6.42

$$\vartheta_{ex}(\tau)=\vartheta_{ex}^{(\mathrm{MOT})}(\tau)=\frac{1}{3}\int_0^{\infty}d\nu\varphi_p^{(\mathrm{MOT})}(\nu)\frac{\tau\theta_\nu}{\kappa_0}\exp\left(-\frac{\tau\theta_\nu}{\kappa_0}\right). \tag{24}$$

As shown in the Appendix, the direct consequences of the occurrence of PFR of reemitted photons in cold samples is a different power-law dependence of escape factors ϑ_{ex}, $\vartheta_{ef}^{(H)}$,

$$\vartheta_{ex}(\tau)\simeq\frac{20\pi}{27}\frac{1}{\tau^{2.5}},\quad \vartheta_{ef}^{(H)}(\tau)\simeq\frac{8\pi^2}{9}\frac{1}{\tau^2}, \tag{25}$$

when $\tau\gg1$. This leads to a formal divergence of the ratio $\vartheta_{ef}^{(H)}(\infty)/\vartheta_{ex}(\infty)$ entering Eq. (21). The asymptotic behavior $\vartheta_{ef}^{(H)}\sim\tau^{-2}$ corresponds to the spectral parameter value $\gamma_{\mathrm{MOT}}=1$ typical for spectral lines with a finite value of photon mean free path. With this γ_{MOT} value in mind, in the case of spherical MOT configurations it is easy to modify Eq. (21) to the form

$$\eta_{\mathrm{MOT}}^{3.5}=\frac{5(1-\rho^3)-3(1-\rho^5)}{\rho^3(1-\rho^2)(5-3\rho^2)}\frac{6\pi}{4.5\sqrt{\tau_A^{(M)}}}$$

$$\times\Lambda_{\mathrm{MOT}}(\tau_A^{(M)}),\quad \Lambda_{\mathrm{MOT}}(\tau)=\frac{4.5\sqrt{\tau}\vartheta_{ex}(\tau)}{6\pi\vartheta_{ef}^{(H)}(\tau)}. \tag{26}$$

This validates the asymptotic value $\Lambda_{\mathrm{MOT}}(\tau=\infty)=1$. The dependence of Λ_{MOT} on the opacity $\tau_A^{(M)}$ of region A is displayed in Fig. 2 (solid line).

C. Correction factors on the curvilinear geometry

Curvilinearity of geometry gives rise to the last type of correction factors. Let us consider the transient situation occurring at early stages, when the whole region A has a zero opacity $\tau=0$, so that photons see the volume Ω with a "hole" A (simulating the region without absorption) inside Ω (Fig. 1). The hole is filled with excited atoms with a density equal to the saturation density n_s^*. The local probability $\vartheta(r)$ for a photon emitted at the point r to freely escape from volume Ω depends on the position r. In order to demonstrate the distinct role of a flat geometry, we investigate the case $\rho\sim1$ under the assumption that photon absorption occurs at the boundary S, in a layer with a small geometrical thickness, $R-r_A\ll R$, but with a rather large opacity, $\tau=\kappa_0 n(R-r_A)\gg1$ (see Fig. 1). The features of $\vartheta(r)$ for a linear geometry ($k=1$) arise from its independence on r. For this reason we can assign to volume Ω the universal linear opacity $\tau=\kappa_0 n(R-r_A)$. The latter statement follows as well from Eq. (18), if one rewrites it as

$$\tau(t=0)=\kappa_0 nR\left(1-\frac{V_A}{V_\Omega}\right)\Rightarrow\tau_L(t=0)=k\kappa_0 n(R-r_A) \tag{27}$$

and sets $k=1$ for a layer. Assuming Eq. (18) to be valid for all types of cells we thus simulated formally the linear geometry.

For curvilinear geometries the above simplification is no longer valid. This can be easily understood from a simple

example: a hollow cylinder as seen from its center is a normal cylinder with optical thickness τ; a photon emitted close to the boundary, on the other hand, sees a plane-parallel layer. It is therefore not surprising that there is a discrepancy between the linear values of opacity evaluated via Eq. (27) and the actual transient values $\tau_a(t=0)$, which determine photon escape and enter into the argument of the effective trapping constant ϑ_{ef}.

Evaluations performed in Appendix D of paper I provide the following results for τ_a:

$$\tau_a(t=0) = \Pi_k \kappa_0 n(R - r_A), \tag{28}$$

with $\Pi_2 = 0.5(1+\ln 4) \simeq 1.19$ for a cylinder and $\Pi_3 = 1+1/3$ for a sphere. We must introduce the correction factor Δ_G into Eq. (27),

$$\tau(t=0) = k\kappa_0 n(R - r_A)(1 + \Delta_G^{(k)}), \tag{29}$$

in such a way that Eqs. (29) and (28) become equal; that leads immediately to *ab initio* determination of the geometrical correction factors: $\Delta_G = -0.4$ for a cylinder ($k=2$) and $\Delta_G = -(5/9)$ for a sphere ($k=3$).

The factors Δ_G describe changes in the escape factor due to a hollow-cylinder or hollow-sphere geometry. Note that the curvilinear cells restore their normal geometrical characteristics at later times of the decay and the geometrical corrections must be terminated as in Eq. (19). Remarkably, in the case of laser focusing in the center of the volume Ω ($\rho \simeq 0$), the size of hollow zones becomes very small and the geometrical correction vanishes. It is therefore reasonable to use the approximation $\Delta_G(\rho) = \rho^k \Delta_G$, as listed in Table I. We underline an important difference between factors Δ_G and Δ_ρ: The correction for the single-mode approach was large when the initially excited region was very small, $\rho=0$, and zero for $\rho=1$. For the geometry modifications, the correction is zero for $\rho=0$ and large for $\rho=1$. It means that the corrections Δ_G and Δ_ρ work practically independently of each other and the final total correction Δ accounting for all possible regimes of decay processes can be taken as their sum (see Table I).

Finally, the above corrections must be carried out for region A as well. Since the laser covers all atoms in V_A, it corresponds formally to the case $\rho \sim 1$ and the correction is accomplished by setting $\Delta_A \equiv \Delta(\rho=1)$, as displayed in Table I.

IV. RESULTS AND DISCUSSION

The system of two equations (11) and (13) provides a comparatively simple tool for analytical evaluation of the nonlinear decay processes under investigation. The factors Δ and Δ_A are summarized in Table I, while the parameter η is determined for the different cases we have considered via Eq. (21) with the spectral parameter $\gamma=0.5$, and via Eq. (26) ($\gamma=1$). Universal algorithms to evaluate the Holstein trapping factors $\vartheta_{ef}^{(H)}(\tau)$ for room-temperature samples are described in Ref. [13]. For MOT conditions, $\vartheta_{ef}^{(H)}(\tau)$ has the form of Eqs. (16), (8), and (9), as discussed in detail in paper II. The escape factors $\vartheta_{ex}(\tau)$ are expressed through Eqs. (17) and (24). It is worth noting that the explicit dependence of

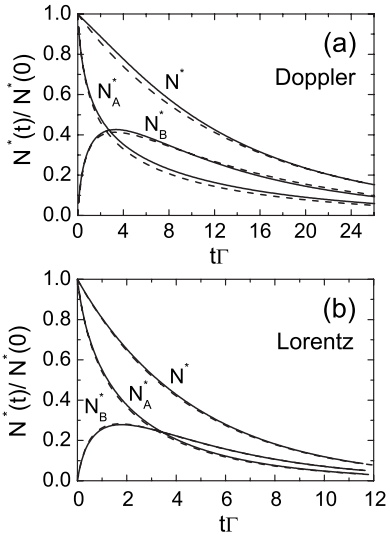

FIG. 3. The case of an infinite cylinder, half-excited ($\rho=0.5$) with opacity $\tau^{(M)}=10$. The normalized decay curves give the total numbers of excited atoms in the whole considered volume Ω (N^*), in laser-excited region A (N_A^*) and in the remaining region B (N_B^*) (see text). The solid lines represent the result of numerical simulations, according to enhanced code of [18]; the dashed lines are the solutions of the reduced equations (11) and (13). (a) Doppler profile case; (b) Lorentz profile case.

$N^*(t)$ on time t is given by the single equation (11), so that it is possible to derive a one-dimensional closed equation for the determination of $N_A^*(t)$ with the initial condition $N_A^*(t=0) = Pn_S^* V_A$. For practical purposes, it is convenient to solve Eq. (13) by exploiting the time dependence of N^* on t,

$$\frac{dN_A^*(t)}{dt} = -\Gamma N^* \vartheta_{ef}^{(H)}(\tau^{(M)}(N^*)) \frac{dN_A^*}{dN^*}. \tag{30}$$

This allows one to treat N_A^* as a function of N^* in Eq. (13) and obtain a solution of $N_A^*(t)$ in parametric form $N_A^*(N^*(t))$.

A. Accuracy determination

We demonstrate the efficiency of our approach by analyzing a few examples of evolution for both the excited-state density and emergent radiation assuming initial and instantaneous saturation of the atomic transition ($P=1$) by the exciting laser pulse. Figures 3 and 4 compare the solutions obtained from our reduced equations (dashed lines) with numerical simulations (solid lines) in the case of a cylindrical geometry $k=2$ (e.g., a configuration typical for plasma and atomic beams) under the CFR assumption. The numerical results are based on an enhanced algorithm described in [18]. Figure 3 corresponds to excitation of an infinite cylinder of radius R and opacity $\tau^{(M)}=10$ by a laser beam of radius $R/2$ ($\rho=0.5$) centered along the cylinder axis. The laser bleaches completely ($P=1$) the region A. We consider two types of spectral lines: Doppler and Lorentz [Figs. 3(a) and 3(b), respectively]. The agreement between our analytical results and the numerical simulation in reproducing the

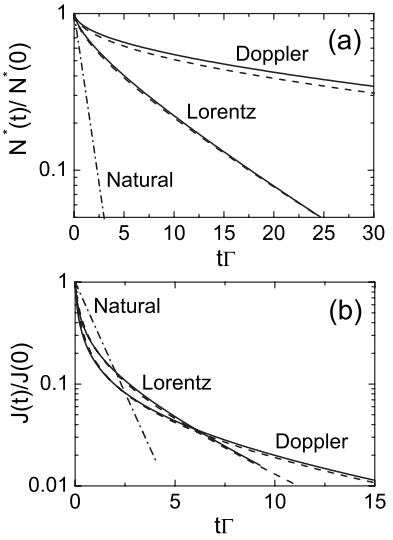

FIG. 4. Entirely excited cylinder ($\rho=1$). The solid and dashed lines represent the results of the numerical [18] and analytical simulations, respectively. (a) Normalized decay curves of the total number N^* of excited atoms for the case of the opacity $\tau^{(M)}=50$. (b) Normalized decay curves of the emerging fluorescence J for the case $\tau^{(M)}=10$. The dash-dotted lines correspond to a decay with the natural lifetime Γ^{-1}.

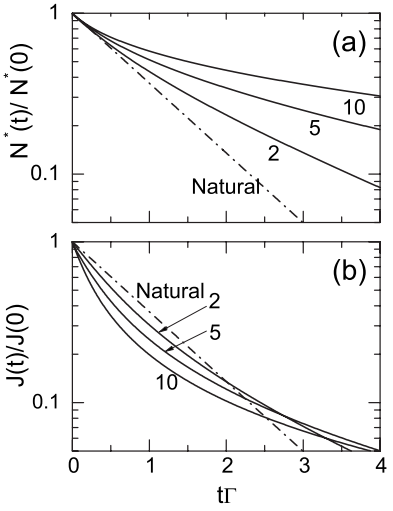

FIG. 5. Illustration of decay processes in a MOT for different values of the opacity $\tau^{(M)}$ as marked close to each curve. (a) Normalized decay of the total number N^* of excited atoms. (b) Behavior of the emerging fluorescence J. The dash-dotted lines correspond to a decay with the natural lifetime Γ^{-1}.

excited atom evolutions N_A^* and N_B^* in zones A and B is better than 5%–7% (we evaluate $N_B^*=N^*-N_A^*$), and in the cylinder as a whole (N^*).

Evaluation of $N^*(t)$ allows us to directly evaluate the behavior of the total flux J of fluorescence emerging from the sample Ω through the obvious relation, $J=-dN^*(t)/dt$. Figure 4 illustrates the decay processes related to an initially fully excited sample of atoms in a cylinder ($\rho=1$). Two different opacity values $\tau^{(M)}=50$ [Fig. 4(a)], 10 [Fig. 4(b)], and two kinds (Doppler and Lorentz) of spectral lines are considered, as specified in the caption. For reference purposes, a dashed line describing decay at the natural rate Γ is also plotted. Finally, the plots in Fig. 5 are evaluated considering a spherical MOT volume ($\rho=1$) and assuming an initial complete bleaching ($P=1$) of the whole MOT volume; three values of opacity, $\tau^{(M)}=2$, $\tau^{(M)}=5$, and $\tau^{(M)}=10$, are considered.

Since fluorescence emission, either time integrated, or, in the case of a pulsed excitation experiment, time resolved, is the quantity which is typically acquired in conventional experiments, it is rather straightforward to conclude that our results for the fluorescence behavior, attained within a fast and accurate analytical approach, can be directly exploited for the interpretation of experimental data.

B. Subnatural decay in magneto-optical trap

From the experimental point of view, an intuitively expected manifestation of RI is the increased effective lifetime $\tau_{\text{eff}}=1/(\Gamma\vartheta_{ef}^{(H)})$ compared to the spontaneous one $(1/\Gamma)$, as can be easily observed upon pulsed excitation. This has been already well demonstrated in a large number of experiments, dealing with thermal samples and, more recently, with cold vapors. The Holstein trapping factor $1/\vartheta_{ef}^{(H)}$ defines the mean number of secondary emission and absorption events occurring before the emitted photons leave the volume Ω. Data on the time behavior of the total number N^* of excited atoms presented in Figs. 4(a) and 5(a) confirm such behavior: The slopes of the N^* curves are smaller than that of the dotted line corresponding to the natural decay of a single isolated atom, which means, for instance, that measuring the decay time in a fluorescence experiment leads to values larger than the natural decay time.

Contrarily to intuitive expectations, the curves shown in Fig. 4(b) and Fig. 5(b) show that the fluorescence flux J can decay with a "subnatural" time constant. In fact, the possibility of such subnatural decay was anticipated in [2,7]. Here, we demonstrate that in the early stages of the decay the flux of the escaping radiation decreases with an effective constant Γ_{eff}, which is larger than the natural decay rate Γ of the resonance level. This intriguing phenomenon occurs due to medium bleaching in the case of total saturation of the vapor volume. At the beginning of the decay optical opacity is zero (the bleaching effect), and photons escape freely. As the process evolves, the density of absorbing atoms increases; RI starts to imprison the photons, thus playing the role of an optical shutter that leads to a strong decrease of the fluorescence signal. As a consequence, an effective subnatural decay is observed.

To the best of our knowledge, such a phenomenon has never been observed in experiments dealing with MOT samples. It can thus be of practical importance to investigate and make some predictions on the subnatural fluorescence emission under typical MOT conditions, such as those (dealing with Cs and Rb MOTs) described in [4]. Briefly, the arrangement of those experiments is as follows. Once the trapping lasers were shut off by means of acousto-optical and mechanical shutters, the trapped cold atoms were excited by a nearly rectangular probe laser pulse with a duration in the 300–1600 ns range. As the repumping laser was left on dur-

ing the whole cycle of the dark period, the trapped atoms were considered to be all in the upper hyperfine level of the ground state ($F=3$ for ^{85}Rb and $F=4$ for Cs). The probe laser frequency was accurately tuned around the line center of the D_2 transition for Cs and Rb, and the saturation parameter s corresponding to the applied laser intensity reached the value 3.

Similar conditions justify well the two-level approach in modeling RI in MOTs. We assume also that the MOT volume has a spherical geometry, i.e., the geometrical parameter in our treatment can be set to $k=3$. The time-dependent structure of the fluorescence signal J is described by the solution of the balance equations (11) and (12), which we rewrite here in a more convenient form,

$$-J=\frac{dN^*}{dt}=-\Gamma\vartheta_{ef}^{(H)}(\tau(N^*))N^*,$$

$$\frac{\tau(N^*)}{\tau^{(M)}}=\left(1-\frac{N^*}{N_s^*}\right)\left(1-\frac{5}{9}\frac{N^*}{N_s^*}\right). \tag{31}$$

A special study of RI trapping factors in a MOT was performed in paper II. It was shown that for sufficiently large values of the probe laser intensities, the Holstein factor $\vartheta_{ef}^{(H)}(\tau)$ can be calculated through Eq. (16), as already discussed in Sec. III. Note that Eqs. (8) and (9) give the parametric dependence of the factor $\vartheta_{ef}^{(H)}(p)$ on the opacity $\tau(p)$. The parameter p plays an important role in geometrical quantization techniques [4,14]. Under MOT conditions, it controls the shape of spectral distributions for emitted photons through Eq. (7). In the present study, omitting all details, we mention only that p directly relates to τ and the ratio $\kappa_0^{(L)}/p$ may be interpreted as a reduced opacity. Large opacity corresponds to small values of p, so that Eq. (7) predicts a $|\nu-\nu_0|^{-6}$ law of wing emission decrease in MOT profiles.

Figure 5(b) shows the calculated MOT fluorescence signals (solid curves) for different values of the opacity τ^M (as indicated by the numbers near the curves). Also shown is the natural decay of the fluorescence with time constant Γ^{-1} (dash-dotted line). The subnatural behavior of the fluorescence decay at times $t<0.5\Gamma^{-1}$ is clearly seen even for opacities as small as $\tau^M=2$, which can be customarily achieved in conventional MOT experiments. Another important observation follows from the comparison between the shapes of the fluorescence signals: The initial slopes of the curves are very sensitive to the opacity, which allows their exploitation for accurate and reliable MOT diagnostics. As a matter of fact, the most informative part of the subnatural signals belongs to early decay times, which do not suffer from the background noise and the poor signal-to-noise ratio typical for analysis of the late decay stages used in the conventional effective lifetime measurement based methods. This circumstance is the distinguishing feature of potential future methods based on the measurement of the subnatural decay, which is expected to lead to more accurate and sensitive evaluation of the MOT operating conditions, in particular its density. Experimental verification of the above phenomena is planned with an alkali MOT.

V. SUMMARY AND CONCLUSIONS

We have analyzed a special class of nonlinear time-dependent integro-differential problems related to radiative energy transfer processes in optically dense vapor samples under both room-temperature and low-temperature conditions, such as those achieved in a MOT. Namely, the evolution of the excited atom population $n^*(\vec{r},t)$ created by a strong and short laser pulse is the main object of our interest. Saturation of the vapor leads to dependence of its effective optical opacity on n^*, and hence the radiation trapping acquires a nonlinear character. We have developed comparatively simple reduced trapping equations allowing for analytical solutions of the excited-state density in the directly excited region, in the fluorescence-excited region, and of the density averaged over the whole vapor sample. We emphasize that having initially derived the reduced equations for somewhat restricted conditions, we succeeded in a substantial extension of their validity through the introduction of three types of correction factors. These corrections account for different regimes of RI decay processes. The actual implementation of the correction factors provides effective means to control the occurrence of competitive regimes at different time intervals. Since the corrections are obtained from *ab initio* principles and are based on solutions of a number of reference problems modeling different aspects of the evolution of excited atoms, they are expected to drastically improve the final accuracy. Comparisons with numerical results show the accuracy to be better than 5%–8% in the cases of the practically relevant Doppler, Lorentz, and Voigt line profiles.

Special attention has been given to analyze vapor samples of curvilinear geometries. In particular, it has been demonstrated that the method of reduced optical depths, which up to now has been employed for plane-parallel geometries of solar and planet atmospheres [3] can be extended with proper corrections to describe nonlinear trapping decay evolution of escaping photons from cylindrical or spherical configurations of vapor cells and MOTs.

We have eventually succeeded as well in modifying our formalism to deal with partial frequency redistribution problems typical for MOT experiments. To the best of our knowledge, no efficient conventional numerical algorithms are available for the prediction of nonlinear radiative dynamics of excited atom population in cold samples. Indeed, on the one hand, Monte Carlo methods fail to work in general nonlinear situations and, on the other hand, traditional treatments of PFR effects based on the piecewise-constant approximation or on the propagator function methods face ill-defined problems in evaluating MOT emission profiles [11].

Thanks to the development of our model, we could simulate the radiation emerging from vapor samples under typical MOT conditions. One of the interesting findings relates to the different asymptotic behavior of trapping factors as compared to the case of room-temperature samples. We demonstrated that bleaching of the MOT volume by the probe laser pulse results in decreasing the effective decay time of the initial part of the fluorescence signal below the natural lifetime. Quite remarkably, the rate constant of this so-called subnatural decay appears to be strongly dependent on the

atom density and can thus be envisioned as a sensitive and reliable diagnostic tool with potential applications in cold and ultracold samples.

ACKNOWLEDGMENTS

We acknowledge the support by the Italian Ministry of Foreign Affairs within the frame of Italo-Russian agreement for Scientific and Technological Cooperation 2002–2004, Contract No RB19, the EU FP6 TOK Project LAMOL (Contract No. MTKD-CT-2004-014228), European Social Fund, and NATO Grant No. EAP.RIG.981378.

APPENDIX

The correction factor η introduced in Sec. III A can be evaluated based on the requirement that the evolution of excited atom density $n^*(\vec{r},t)$ at late times of afterglow should be correct, i.e., the n^* decay is ruled by the fundamental mode characteristics: $n^*(\vec{r},t)=Cn_H^*(r)\exp(-\Gamma\vartheta_{ef}^{(H)}t)$, where C is some constant. The space profile $n_H^*(r)\simeq(1-r^2/R^2)^\gamma$ of the fundamental mode is determined by the spectral parameter γ while the decay constant $\vartheta_{ef}^{(H)}=\vartheta_{ef}^{(H)}(\tau^{(M)})$ is the so-called Holstein trapping factor [13] for absorbing media with opacity $\tau^{(M)}$. The total atom number $N_i^*(t)$ in different parts of the vapor volume can be evaluated as $N_i^*(t)\simeq CN_i^*\exp(-\Gamma\vartheta_{ef}^{(H)}t)$, which reduces Eq. (13) to a simple equality

$$-\vartheta_{ef}^{(H)}(\tau^{(M)})N_A^*=-\vartheta_{ef}^{(H)}(\tau_A^{(M)})N_A^*+(N^*-N_A^*)\frac{1}{\eta}\vartheta_{ex}(\tau_A^{(M)}\eta), \tag{A1}$$

with N_A^* and N^* to be expressed via Eq. (22). Equation (A1) allows for a straightforward determination of the η values in the form of Eq. (21) if one takes into account the following factorization properties of escape factors at large opacities $\tau^{(M)}$ and $\tau_A^{(M)}$ (see details in paper I):

$$\vartheta_{ef}^{(H)}(\tau^{(M)})/\vartheta_{ef}^{(H)}(\tau_A^{(M)})=\left(\frac{\tau_A}{\tau}\right)^{2\gamma}=\rho^{2\gamma},$$

$$\vartheta_{ex}(\eta\tau_A)\eta^{-1}=\vartheta_{ex}(\tau_A)\eta^{-1-2\gamma}. \tag{A2}$$

Note that for the sake of simplicity we have arranged the multipliers in a special manner to obtain an uniform normalization $\Lambda_k(\tau_A^{(M)}=\infty)=1$.

The asymptotic behavior $\vartheta(\tau\to\infty)\sim\tau^{-2\gamma}$ mentioned in Sec. III A and ensuring the validity of relations (A2) are well known for traditional emission spectral lines at room-temperature conditions. In MOT experiments, however, emission and absorption profiles have quite different shapes (see Sec. III B) at high opacities so that escape factor asymptotes must be carefully considered. Starting from the Holstein function $\vartheta_{ef}^{(H)}(\tau)$ determined by Eqs. (8), (9), and (16), one immediately finds a simple relation between the dimensionless parameter $\tilde{p}=p/\kappa_0^{(M)}$ (the so-called inverse reduced opacity [13]) and the opacity τ when τ is large, $\tilde{p}\tau=\pi$. The expansion of the function $V_p(\nu)$, Eq. (7), over the small parameter $\tilde{p}$ $(\tau\to\infty)$ transforms integral (8) to the asymptote

$$\lambda_p^{-1}\simeq\frac{3\tilde{p}^2}{\pi}\int_{-\infty}^{\infty}\frac{d\nu}{(1+\nu^2)^3}=\frac{9p^2}{8},\quad \tilde{p}\tau=\pi,\quad \tau\to\infty, \tag{A3}$$

which is equal to Eq. (25).

Considering Eq. (24), it is clear that when $\tau\to\infty$, the main contribution to the integral over the frequency ν comes from large values of ν (where $\tau\theta_p\leq 1$). For this reason, one may set $1+\nu^2\simeq\nu^2$ in both $\varphi_p^{(\mathrm{MOT})}(\nu)$ [Eq. (7)] and $\kappa_{\mathrm{MOT}}(\nu)$ [Eq. (2)] profiles and thus reduce Eq. (24),

$$\vartheta_{ex}^{(\mathrm{MOT})}(\tau)=\frac{\lambda_p}{3\pi}\int_{-\infty}^{\infty}\frac{d\nu\tau}{\nu^4\tilde{\varphi}(\nu)}\exp(-\tau\nu^{-2}),$$

$$\tilde{\varphi}(\nu)=1-\frac{1}{\tilde{p}\tau\nu^2}\arctan(\tilde{p}\tau\nu^2). \tag{A4}$$

A natural scaling $\nu=x\sqrt{\tau}$ with the following transformation of the integration variable $x=1/y$ yields

$$\vartheta_{ex}^{(\mathrm{MOT})}(\tau)=\frac{2\lambda_p}{3\pi\sqrt{\tau}}\int_0^{\infty}\frac{dyy^2}{\tilde{\varphi}(1/y)}\exp(-y^2),\quad \tau\to\infty. \tag{A5}$$

Having in mind that $\tilde{p}\tau=\pi$, finding the numerical value 1.127 for the integral over y, and accounting for the asymptote (A3), we obtain the result presented in Eq. (25).

[1] L. M. Biberman, V. S. Vorobjev, and I. T. Yakubov, *Kinetics of Nonequilibrium Low-Temperature Plasma* (Plenum, New York, 1987).
[2] A. F. Molisch and B. P. Oehry, *Radiation Trapping in Atomic Vapours* (Oxford University Press, Oxford, 1998).
[3] V. V. Ivanov, *Transfer of Radiation in Spectral Lines*, NBS Special Publication No. 385 (U.S. GPO, Washington, DC, 1973).
[4] N. N. Bezuglov, A. F. Molisch, A. Fioretti, C. Gabbanini, F. Fuso, and M. Allegrini, Phys. Rev. A **68**, 063415 (2003).
[5] G. Labeyrie, D. Delande, C. Muller, C. Miniatura, and R. Kaiser, Phys. Rev. A **67**, 033814 (2003).
[6] O. Kaufmann, A. Ekers, K. Bergmann, N. Bezuglov, K. Miculis, M. Auzinsh, and W. Meyer, J. Chem. Phys. **119**, 3174 (2003).
[7] T. Stacewicz, T. Kotowsky, P. Wievior, and J. Chorazy, Opt. Commun. **100**, 99 (1993).
[8] N. N. Bezuglov, A. N. Klucharev, A. F. Molisch, M. Allegrini, F. Fuso, and T. Stacewicz, Phys. Rev. E **55**, 3333 (1997).
[9] T. Walker, D. Sesko, and C. Wieman, Phys. Rev. Lett. **64**, 408 (1990).
[10] K. Ellinger and J. Cooper, Phys. Rev. A **55**, 4351 (1997).

[11] A. Fioretti, A. F. Molisch, J. H. Müller, P. Verkerk, and M. Allegrini, Opt. Commun. **149**, 415 (1998).
[12] G. Labeyrie, E. Vaujour, C. A. Muller, D. Delande, C. Miniatura, D. Wilkowski, and R. Kaiser, Phys. Rev. Lett. **91**, 223904 (2003).
[13] N. N. Bezuglov, A. F. Molisch, A. N. Klucharev, F. Fuso, and M. Allegrini, Phys. Rev. A **57**, 2612 (1998).
[14] N. N. Bezuglov, A. K. Kazansky, F. Fuso, and M. Allegrini, Phys. Rev. A **63**, 042703 (2001).
[15] N. N. Bezuglov, A. K. Kazansky, A. N. Klucharev, K. Miculis, M. Allegrini, and F. Fuso, Opt. Spectrosc. **95**, 631 (2003)[Opt. Spektrosk. **95**, 675 (2003)].
[16] N. N. Bezuglov, A. Ekers, O. Kaufmann, K. Bergmann, F. Fuso, and M. Allegrini, J. Chem. Phys. **119**, 7094 (2003).
[17] A. Streater, J. Cooper, and W. Sandle, J. Quant. Spectrosc. Radiat. Transf. **37**, 151 (1987).
[18] A. F. Molisch, B. P. Oehry, W. Schupita, and G. Magerl, Opt. Commun. **118**, 520 (1995).
[19] C. van Trigt, Phys. Rev. **181**, 97 (1969); C. van Trigt, Phys. Rev. A **1**, 1298 (1970); C. van Trigt, *ibid.* **4**, 1303 (1971); C. van Trigt, *ibid.* **13**, 726 (1976).
[20] T. Holstein, Phys. Rev. **72**, 1212 (1947); **83**, 1159 (1951).
[21] M. G. Payne, J. E. Talmage, G. S. Hurst, and E. B. Wagner, Phys. Rev. A **9**, 1050 (1974).
[22] I. S. Gradstein and I. M. Ryzhik, *Tables of Series, Products and Integrals* (Academic, New York, 1994).